Differentiation of Normal and Cancer Cell Adhesion on Custom Designed Protein Nanopatterns

Utku Horzum, Berrin Ozdil, and Devrim Pesen-Okvur*

Department of Molecular Biology and Genetics, Izmir Institute of Technology, 35430 Urla/Izmir, Turkey

🅂 Supporting Information

ABSTRACT: Cell adhesion to the extracellular matrix is deregulated in metastasis. However, traditional surfaces used to study cell adhesion do not faithfully mimic the in vivo microenvironment. Electron beam lithography (EBL) is able to generate customized protein nanopatterns. Here, we used an

EBL-based green lithography approach to fabricate homogeneous and gradient, single (fibronectin, K-casein) and double (fibronectin, laminin) active component protein nanopatterns with micrometer scale spacing to investigate differences in adhesion of breast cancer cells (BCC) and normal mammary epithelial cells (NMEC). Our results showed that as expected, in contrast to NMEC, BCC were plastic: they tolerated nonadhesion promoting regions, adapted to flow and exploited gradients better. In addition, the number of focal adhesions but not their area appeared to be the dominant parameter for regulation of cell adhesion. Our findings also demonstrated that custom designed protein nanopatterns, which can properly mimic the in vivo microenvironment, enable realistic distinction of normal and cancerous cell adhesion.

KEYWORDS: Focal adhesion, fibronectin, laminin, nanopattern, cancer, electron beam lithography
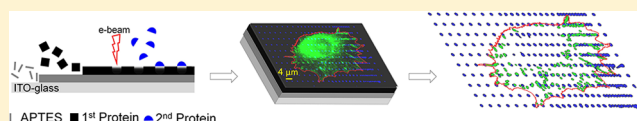
The microenvironment of cells plays key roles in metastasis, angiogenesis, tumorigenesis, embryonic development, tissue homeostasis, atherosclerosis, and wound healing. Studies on cell adhesion to extracellular matrix routinely use uniformly coated surfaces that do not truly represent the extracellular matrix in vivo that is comprised of nanometer scale adhesive patches separated by micrometer scale spacing.[1−5] Focal adhesions (FAs) are protein compositions involved in the biomechanical and biochemical interactions of cells with the extracellular matrix. The extracellular and intracellular parts of a FA are extracellular matrix proteins (e.g., fibronectin, laminin) and cytoskeletal proteins (e.g., actin, vinculin), respectively.[5−10] Although there are significant cell adhesion studies that use surfaces fabricated to mimic the extracellular matrix at the nano- and micrometer scales,[11−24] the regulation of cell morphology and FA features by the spatial arrangement of the extracellular matrix remains incompletely understood.[15,21] Furthermore, there are no studies comparing adhesion of normal and cancer cells on nanopatterns. Cell adhesion to the extracellular matrix is one of the major processes that is disturbed in cancer cells.[25] For instance, expression levels of molecules that mediate cell-to-matrix adhesion such as integrins are known to be altered in cancer cells.[26] Altered adhesion appears to favor metastasis and therefore a deeper understanding of the differences in cell adhesion between normal and cancer cells is desired.[27,28] Among known patterning techniques, electron beam lithography offers considerable practical and technical advantages that provide well-controlled nanofabricated biomimetic surfaces with defined pattern geometries.[29−32] Previous work showed that vinculin and cytoskeletal organization are modulated by the size and shape of surface ligand nanopatterns.[24,33] Here, we present the first comparative and quantitative analysis of cell morphology and

focal adhesions of normal mammary epithelial (NMEC) and breast cancer cells (BCC) on custom designed protein nanopatterns. We used the MDA-MB-231 and MCF10A cell lines to represent highly invasive and normal mammary epithelial cells, respectively, because they are the corresponding most extensively used model cell lines.[12,34−37] Quantitative comparisons were performed as a function of micrometer scale spacing of homogeneous and gradient fibronectin nanopatterns on K-casein and laminin backgrounds under static and/or flow conditions.

Results and Discussion. *Cell Morphology on SAC.* To mimic the in vivo organization of the extracellular matrix, nanometer scale protein patterns with micrometer scale spacing were fabricated using a previously described electron beam lithography based approach[33] (Supporting Information Figure S1). Briefly, protein coated ITO-glass surfaces were exposed to an electron beam and the exposed parts were subsequently backfilled with a second protein of interest. BCC and NMEC were cultured on single active component (SAC) surfaces that were realized as fibronectin nanopatterns on a K-casein background and on control surfaces that were uniformly coated with either fibronectin or K-casein. Cells were stained for actin and FAs were identified by immunofluorescence staining of vinculin, a well-established FA marker. Fluorescence images were analyzed to determine cell morphology and FA features (Figure 1).

Representative images are shown in Figure 2a. Cell areas for both cell types on SAC surfaces and on K-casein control surfaces were similar to each other and smaller than those on fibronectin
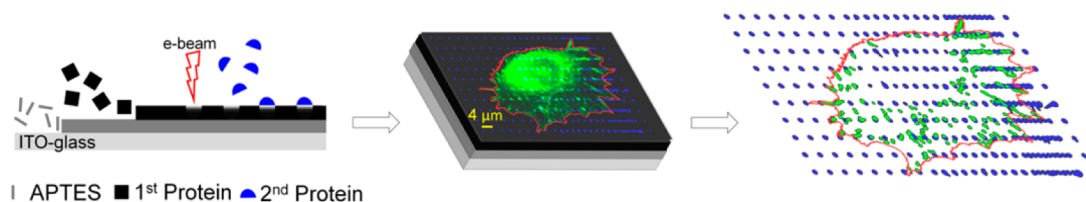
Figure 1. Comparative and quantitative study of cell adhesion on transparent ITO-glass by EBL-based green lithography approach. ITO-glass surfaces were functionalized with APTES (3-aminopropyl triethoxy-silane) before coating with the first protein of interest. Protein-coated ITO-glass was exposed to a focused electron beam and backfilled with a second protein of interest. Cells were cultured on custom protein nanopatterns before immunofluorescence staining. Fluorescence images were analyzed to determine cell morphology and FA features as a function of nanopatterns.

control surfaces (Figure 2b). The areas of BCC and NMEC on SAC were on average 51% and 39% smaller than those on fibronectin control surfaces, respectively. Areas of BCC were significantly greater than those of NMEC on fibronectin control and SAC surfaces with 4 and 8 μm spacing ($p < 0.05$). Thus, BCC tolerated nonadhesive regions better than NMEC as they occupied larger areas on SAC surfaces.

BCC were asymmetric on both control and SAC surfaces (Figure 2c). Their asymmetry was highest on fibronectin control surfaces and decreased as the spacing between fibronectin nanodots increased. BCC were 2-, 1.4-, and 1.5-fold more asymmetric than NMEC on fibronectin control and SAC surfaces with 2 and 4 μm spacing, respectively ($p < 0.05$). Aspect ratios of NMEC were virtually constant on both control and SAC surfaces. These results indicated that while NMEC preserved their aspect ratio on SAC, BCC responded to SAC by decreasing their asymmetry.

FAs on SAC Surfaces. FAs of BCC and NMEC on were assessed on SAC surfaces. Number of FAs per cell on fibronectin nanodots decreased as the spacing between nanodots increased on SAC surfaces for both cell types (Figure 2d). The number of FAs per cell on the K-casein background was virtually constant for both cell types. The number of FA per cell on fibronectin nanodots with 4 and 8 μm spacing were fewer than those off fibronectin nanodots for both cell types ($p < 0.05$, †, ‡).

Significant differences between cell types were observed on fibronectin control surfaces and on SAC surfaces with 4 and 8 μm spacing. The number of FAs per cell on fibronectin control surfaces was 1.8 fold higher for BCC in comparison to NMEC ($p < 0.05$, *). In addition, the number of FA per cell on the K-casein background on SAC surfaces with 4 and 8 μm spacing was 1.5 and 1.7 fold higher for BCC than those for NMEC ($p < 0.05$, *). These results showed that BCC cells formed more FAs on the K-casein background of SAC surfaces than NMEC.

Areas of FAs on fibronectin nanodots increased as the spacing between fibronectin nanodots increased on SAC surfaces for both cell types (Figure 2e). The areas of FAs on the K-casein background were virtually constant for both cell types. FAs on fibronectin nanodots were 1.8−1.9-fold larger than those on the K-casein background for both cell types ($p < 0.05$, †, ‡). Although FAs of BCC were smaller than those of NMEC on fibronectin control surfaces ($p < 0.05$, *), FAs of BCC on the K-casein background were larger than those of NMEC for 2 and 4 μm spacing ($p < 0.05$, *). These results showed that BCC cells could form larger FAs off fibronectin nanodots on SAC surfaces than NMEC.

Analysis of the number and area of FAs on SAC surfaces revealed that as the spacing between fibronectin nanodots increased on SAC surfaces, cells tended to form fewer but larger FAs on fibronectin nanodots. The FAs on the K-casein background reflect first, the background introduced with the

extracellular matrix components which are present in the serum of the culture media and which are secreted by the cells. Second, and more importantly, the FAs reflect the requirement of cells for adhesion promoting surfaces. Here BCC cells were more flexible than NMEC as they formed more and larger FAs than NMEC cells on the K-casein background. The results of FA analysis were consistent with the results of cell area analysis, that is, BCC tolerated nonadhesive regions better than NMEC on SAC surfaces.

FAs start as small circular structures and evolve into large fibrillar ones. Circularity versus size correlation was consistent with the maturation of FAs (Supporting Information Figure S2a). In addition, the formation of FAs on SAC surfaces with various spacing was not stochastic. For example, the total area of fibronectin was 5% of the total patterned area whereas the number of FAs on fibronectin nanodots was 33% of the total FAs per cell for 4 μm spacing. In addition, FAs on fibronectin were larger than those on the K-casein background. Thus, cells could form FAs on both the fibronectin nanodots and the K-casein background but FAs matured only on fibronectin nanodots.

Cell Morphology on DAC. BCC and NMEC were cultured on double active component (DAC) surfaces which were realized as fibronectin nanopatterns on a laminin background and on control surfaces which were uniformly coated with either fibronectin or laminin. Representative images are shown in Figure 3a. BCC occupied larger areas on fibronectin control compared to DAC and laminin control surfaces ($p < 0.05$) whereas NMEC occupied similar areas on both control and DAC surfaces (Figure 3b). The areas of BCC on DAC surfaces were on average 45% and 15% smaller than those on fibronectin and laminin control surfaces, respectively. Areas of NMEC on DAC surfaces were on average 23% and 22% smaller than those on fibronectin and laminin control surfaces, respectively. Areas of both cell types on laminin control surfaces were 1.2-fold larger than those on K-casein control surfaces. Areas of BCC on fibronectin control surfaces were 1.6-fold larger than those on laminin surfaces. These results confirmed that both fibronectin and laminin promoted cell adhesion in contrast to K-casein. Furthermore, the results indicated that fibronectin was a better cell adhesion promoter than laminin for BCC but not NMEC. This could be in part due to the differential expression levels of integrins that bind fibronectin and laminin in BCC and NMEC.[38]

BCC were similarly asymmetric on both control and DAC surfaces (Figure 3c). Aspect ratios of NMEC were virtually constant on fibronectin control and DAC surfaces. However, NMEC were 1.7-fold more asymmetric on laminin than on fibronectin control surfaces. BCC were significantly more (1.5−2-fold) asymmetric than NMEC on fibronectin control and all DAC surfaces ($p < 0.05$). These results indicated that both cell types preserved their asymmetry on DAC surfaces.

In contrast to SAC surfaces, both cell types occupied larger areas on DAC surfaces as expected since both fibronectin
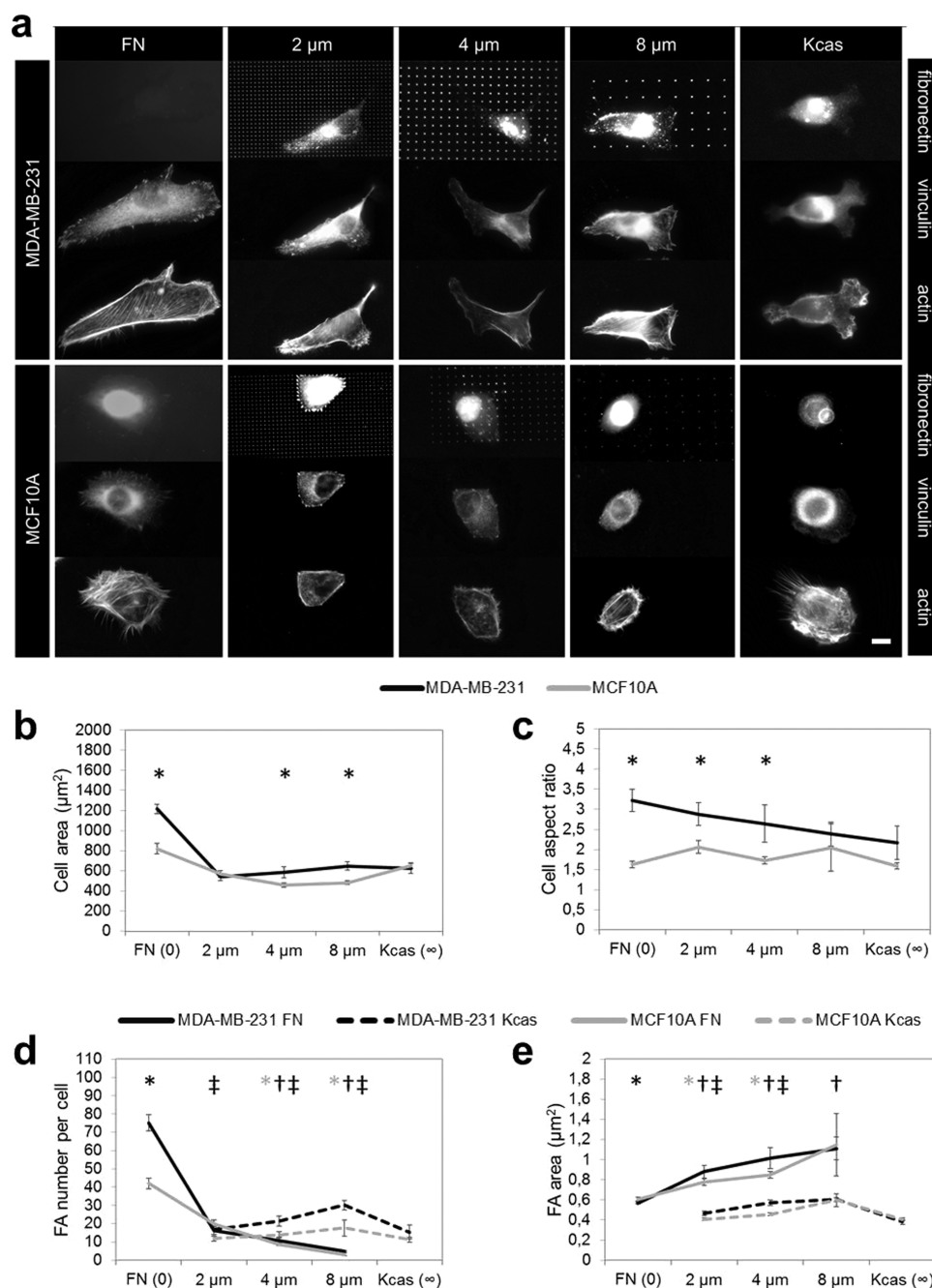
Figure 2. BCC tolerate nonadhesive regions better than NMEC on SAC surfaces. (a) Representative images of cultured BCC and NMEC on SAC surfaces. Scale bar, 8 μm. (b) Cell area, (c) cell aspect ratio, (d) FA number per cell, and (e) FA area on SAC surfaces. Black and gray asterisks (*) indicate significant differences between cell types for fibronectin and on K-casein, respectively at $p < 0.05$. Single cross (†) and double cross (‡) indicate differences between fibronectin (FN) and K-casein (K-cas) for BCC and NMEC, respectively at $p < 0.05$.

and laminin promote cell adhesion. The aspect ratios of NMEC were similar between SAC and DAC surfaces. Yet, aspect ratios of BCC were higher on SAC than on DAC surfaces with 8 μm spacing and on laminin than on K-casein control surfaces.

FAs on DAC Surfaces. For both BCC and NMEC on DAC surfaces, the number of FAs per cell on fibronectin nanodots and on the laminin background decreased and increased, respectively, as the spacing between fibronectin nanodots increased (Figure 3d). For both BCC and NMEC, the number of FAs on fibronectin nanodots was higher than those on the laminin background for 2 μm spacing whereas more FAs formed on the

laminin background for 4 and 8 μm spacing ($p < 0.05$, †, ‡). Differences between cell types were observed on DAC surfaces with 2 and 4 μm spacing: the number of FAs per cell on fibronectin nanodots was 2.3- and 1.6-fold higher for BCC than for NMEC ($p < 0.05$, *).

In comparison to SAC surfaces, the number of FAs per cell off fibronectin nanodots was higher on DAC surfaces for both cell types. This was expected because laminin also promotes cell adhesion. In addition, the number of FAs per cell on fibronectin nanodots was higher on DAC than on SAC for both cell types, suggesting adhesion to laminin can enhance adhesion to fibronectin.
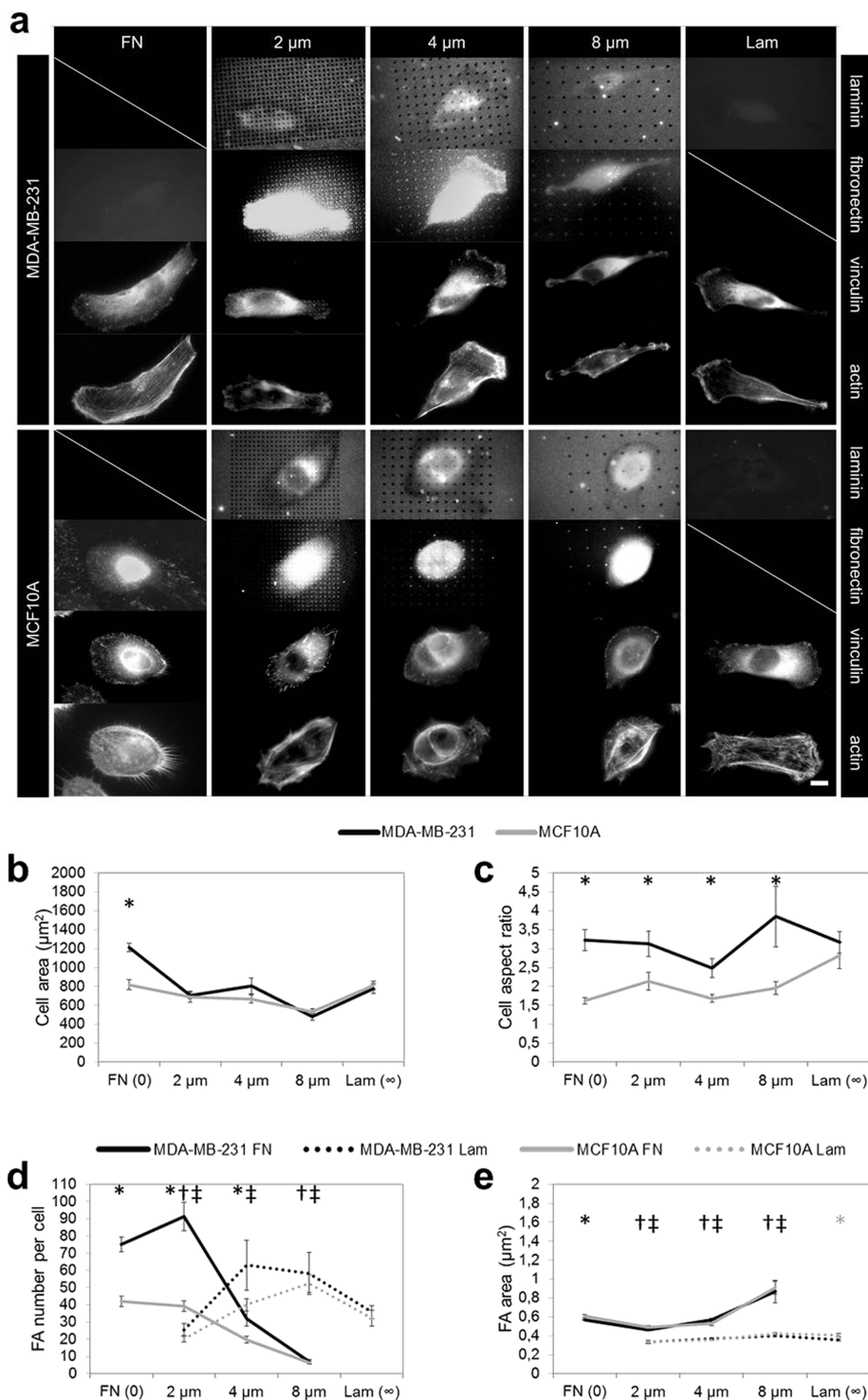
Figure 3. DAC surfaces enhance cell adhesion. (a) Representative images of cultured BCC and NMEC on DAC surfaces. Scale bar, 8 μm. (b) Cell area, (c) cell aspect ratio, (d) FA number per cell, and (e) FA area on DAC surfaces. Black and gray asterisks (*) indicate significant differences between cell types for fibronectin (FN) and on laminin (Lam), respectively at $p < 0.05$. Single cross (†) and double cross (‡) indicate differences between fibronectin and laminin for BCC and NMEC, respectively, at $p < 0.05$.

Areas of FAs on fibronectin nanodots increased as the spacing between fibronectin nanodots increased on DAC surfaces for both cell types (Figure 3e). Areas of FAs on the laminin background were virtually constant for both cell types. FAs on fibronectin nanodots were 1.4- to 2.2-fold larger than those on the laminin background for both cell types ($p < 0.05$, †, ‡). FAs of BCC were smaller than those of NMEC on fibronectin and laminin control surfaces ($p < 0.05$, * *). Circularity versus size

correlation was the same on DAC surfaces as on SAC surfaces (Supporting Information Figure S2b).

In comparison to SAC surfaces, the areas of FAs on fibronectin nanodots were smaller on fibronectin nanodots on DAC surfaces for both cell types. In addition, areas of FAs on the laminin background of DAC surfaces were smaller than those on the K-casein background of SAC surfaces. These results suggested that when cell adhesion promoting regions were limited, as in the

case of SAC surfaces, cells could focus their resources to enlarging FAs on the available cell adhesion promoting regions. However, when both fibronectin and laminin were available, resources of cells could be more equally distributed and cells could form more but smaller FAs. This was also in agreement with more FAs per cell forming on the laminin background than on the K-casein background.

Differences between BCC and NMEC were more pronounced on SAC surfaces than on DAC surfaces as expected. Here, SAC surfaces mimicked the condition where the microenvironment does not provide ample adhesion promoting options. In this case, BCC could adhere better than NMEC. Such plasticity is likely to favor cell survival.

Cell Morphology on SAC under Flow. BCC and NMEC were introduced under flow to single active component (SAC) surfaces that were realized as fibronectin nanopatterns on a K-casein background and on control surfaces that were uniformly coated with either fibronectin or K-casein. The shear stress applied was 0.02 dyn/cm ^{2}, mimicking interstitial flow.[39] Representative images are illustrated in Figure 4a.

Under flow, areas of BCC were 2-fold larger than those of NMEC on fibronectin control surfaces and SAC surfaces with 2 and 4 μm spacing ($p < 0.05$) (Figure 4b). No cells attached to K-casein surfaces. In comparison to static conditions, areas of BCC and NMEC on fibronectin control surfaces were 23% and 41% smaller under flow ($p < 0.05$), respectively (Supporting Information Figure S3a). The areas of NMEC also decreased on SAC with 2 and 4 μm spacing under flow ($p < 0.05$). However, the areas of BCC on SAC with 2 and 4 μm spacing under flow were larger than those under static conditions. Thus, the presence of flow on SAC surfaces regulated cell area of BCC and NMEC in an opposite manner. Areas of NMEC decreased with flow as expected whereas areas of BCC increased with flow. The ability to increase area of cell adhesion under flow is likely to favor dissemination of BCC.

As expected, both types of cells were more symmetric under flow in comparison to static conditions. BCC were more asymmetric than NMEC on fibronectin control and SAC surfaces with 2 and 8 μm spacing under flow ($p < 0.05$) (Figure 4c).

FAs on SAC Surfaces under Flow. The number of FAs per cell on fibronectin nanodots and on the K-casein background decreased and increased, respectively, as the spacing between fibronectin nanodots increased on SAC surfaces under flow for both cell types (Figure 4d). The number of FAs per cell on fibronectin nanodots with 8 μm spacing was fewer than those off fibronectin nanodots for both cell types whereas the opposite was observed for 2 μm spacing. In addition, BCC formed more FAs than NMEC on K-casein background of SAC surfaces with 4 μm spacing ($p < 0.05$, †, ‡). Significant differences between cell types were observed on both fibronectin control and SAC surfaces. Here, the number of FAs per cell on fibronectin control surfaces was 3.25-fold higher for BCC than NMEC ($p < 0.05$, *). The number of FAs per cell on fibronectin was higher for BCC than for NMEC for 4 and 8 μm spacing whereas the number of FAs on the K-casein background was higher for BCC than for NMEC on all SAC surfaces ($p < 0.05$, *). In contrast to static conditions, BCC and NMEC formed more and fewer FAs on fibronectin control surfaces, respectively ($p < 0.05$). BCC also formed more FAs than NMEC on the K-casein background of SAC surfaces with 2, 4, and 8 μm spacing ($p < 0.05$).

For both cell types on SAC surfaces under flow, the areas of FAs on fibronectin increased as the spacing between fibronectin nanodots increased; the areas of FAs on the K-casein background

were virtually constant (Figure 4e). FAs of BCC were larger than those of NMEC on fibronectin control and on the K-casein background of SAC with 2 μm spacing ($p < 0.05$, *). In contrast to the static conditions, under flow, (i) both cell types formed smaller FAs on fibronectin control surfaces and on fibronectin nanodots of SAC with 2 spacing; (ii) FAs of both cell types on the K-casein background of SAC with 2 and 8 μm spacing were smaller; and (iii) FAs of BCC on fibronectin for SAC with 4 and 8 μm spacing were smaller ($p < 0.05$).

The analysis of the number and area of FAs on SAC surfaces under flow revealed that flow induced an increase in the number of FAs and a decrease in the area of FAs in both cell types yet the changes for BCC were more pronounced. Number of FAs on fibronectin nanodots per cell increased to 220% and 138% for BCC and NMEC, respectively, while areas of FA on fibronectin nanodots decreased to 62% and 79% for BCC and NMEC, respectively (Supporting Information Table S1).

The number density of FAs of both cell types was not polarized on fibronectin control surfaces under static conditions as expected (Supporting Information Figure S4a). However, under flow the number density of FAs was polarized for NMEC but not BCC (Supporting Information Figure S3b). Thus, the number of FAs per area was higher upstream of flow for NMEC only, suggesting that NMEC but not BCC tended to resist the flow once they adhere to the surface. On SAC surfaces without flow, number densities of FAs for both cell types were polarized showing the presence of an inherent polarization induced by SAC nanopatterns (Supporting Information Figure S5a). Kurtosis values showed that the inherent polarization varied such that it was most peaked for FAs of BCC on fibronectin of SAC and flattest for FAs of NMEC on K-casein of SAC (Supporting Information Table S2). On K-casein control surfaces, polarization of FA number density and area were scattered (Supporting Information Figure S4e,f). Thus, inherent polarization was higher for BCC and was driven by FAs on fibronectin nanodots, not the K-casein background of SAC. Importantly, on SAC surfaces with flow, number densities of FAs on fibronectin nanodots and on the K-casein background were higher upstream of flow for both cell types suggesting that the inherent polarization was aligned with the flow (Figure 4f).

The areas of FAs of NMEC but not BCC were polarized on fibronectin control surfaces under static conditions: BCC formed similarly sized FAs whereas NMEC formed larger FAs at one side of the cell (Supporting Information Figure S4b). Thus, even though NMEC did not polarize the density of their FAs, they did polarize the size of their FAs. This was probably because cells were searching for other cells as NMEC tend to form clusters in standard cell culture. Areas of FAs of both cell types on SAC surfaces without flow were polarized whereas under flow all FAs were of similar sizes as they were on fibronectin control surfaces under flow (Figure 4g, Supporting Information Figures S3c and S5b). Thus, flow removes differences in areas of FAs for both cell types.

Overall, flow modulates morphology of BCC and NMEC in an opposite manner. Flow also changed the FA features of both cell types but the changes were more prominent for BCC, suggesting a better adaptation response to flow.

Interestingly, both FAs on the K-casein background under flow and FAs on the laminin background under static conditions were more numerous than FAs on the K-casein background under static conditions. Thus, the presence of an adhesion promoting protein on the background or the physical stimulation of low shear stress can both induce FA formation in cells.
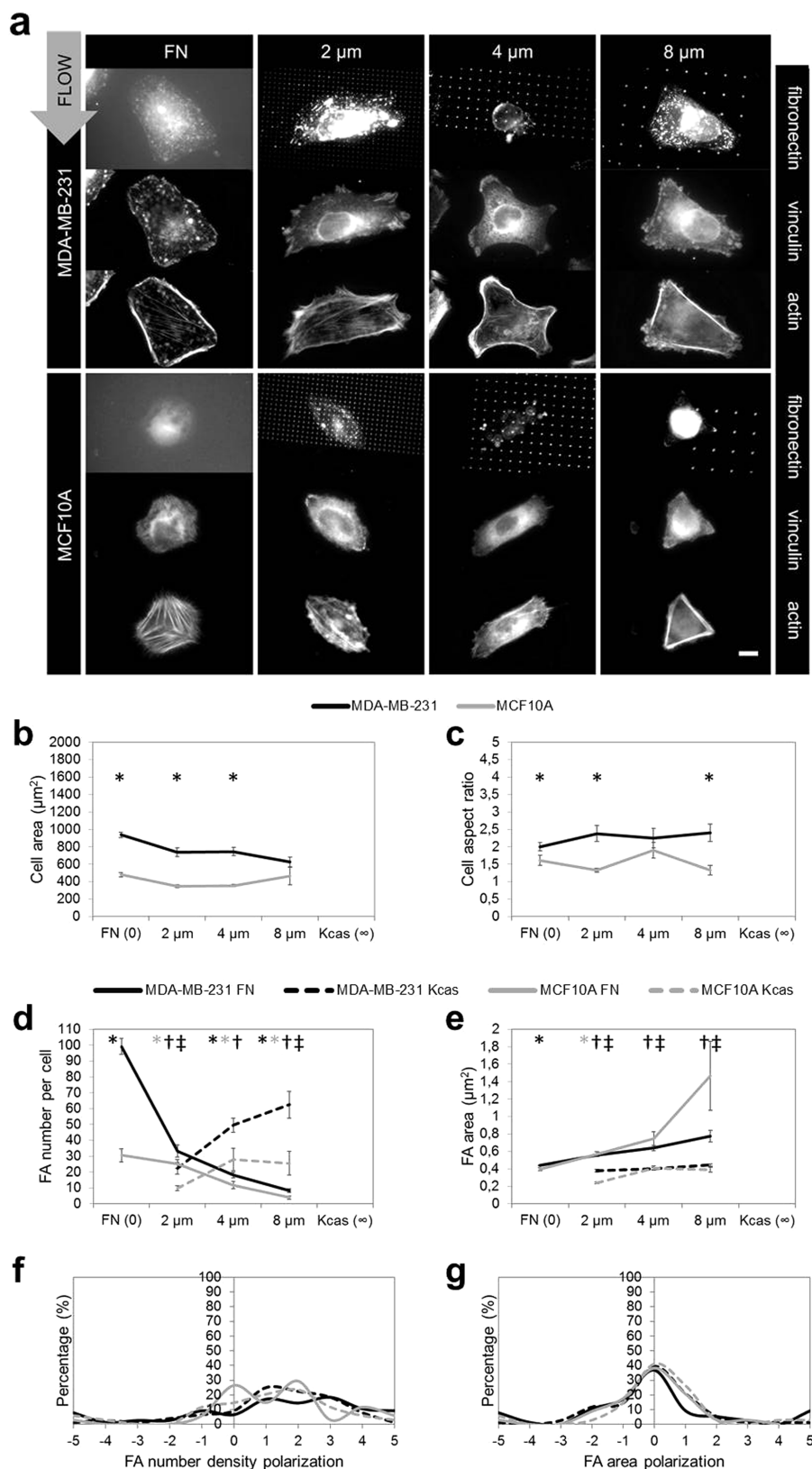
Figure 4. BCC adapt to flow better than NMEC. (a) Representative images of cultured BCC and NMEC on SAC surfaces under flow. Arrow shows the direction of flow. Scale bar, 8 μm. (b) Cell area, (c) cell aspect ratio, (d) FA number per cell, (e) FA area, (f) FA number density polarization, and (g) FA area polarization. Black and gray asterisks (*) indicate significant differences between cell types for fibronectin and on K-casein, respectively at $p < 0.05$. Single cross (†) and double cross (‡) indicate differences between fibronectin and K-casein for BCC and NMEC, respectively at $p < 0.05$. X-axis in (f,g) shows the degree of polarization; negative and positive values represent polarization against and along the flow direction.
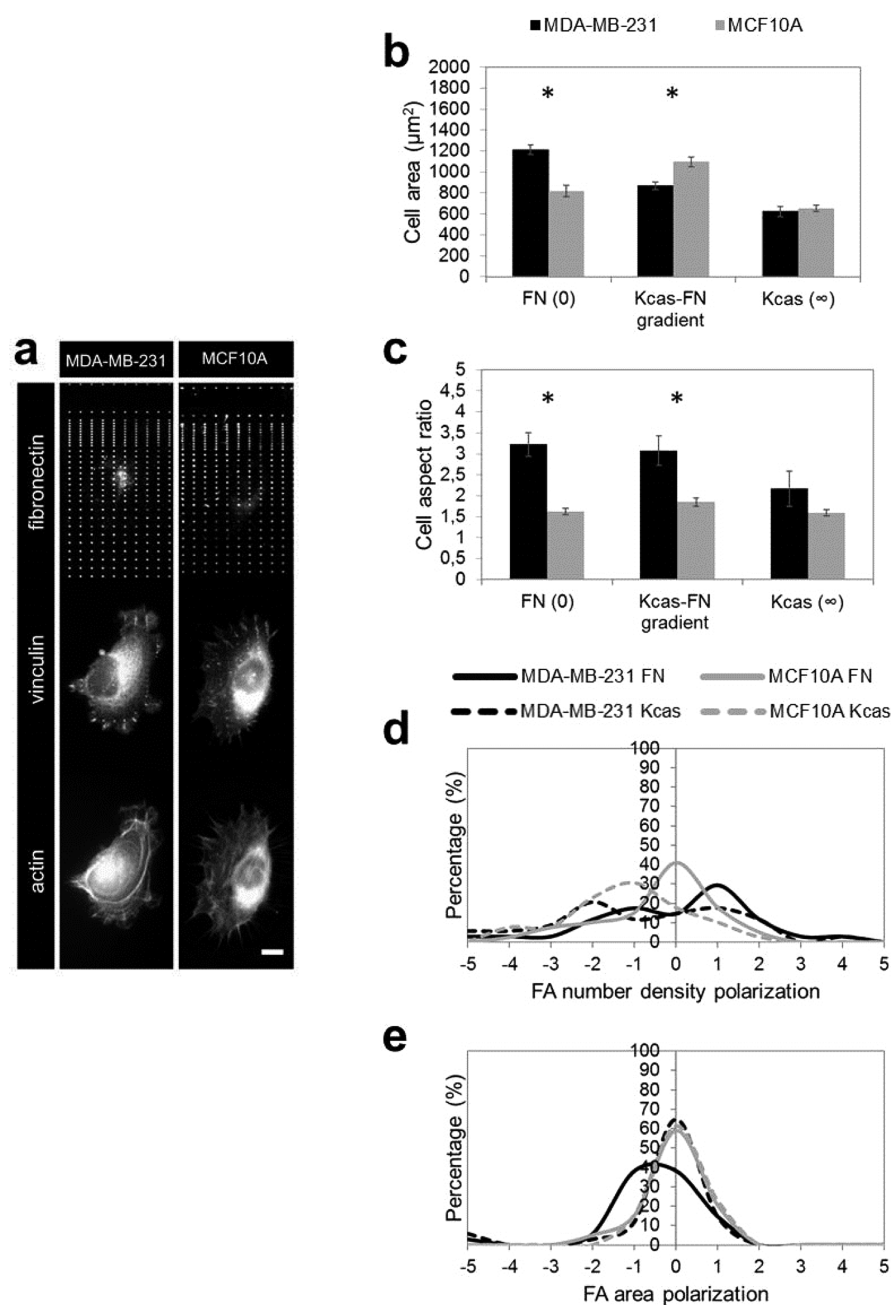
Figure 5. BCC exploits gradient SAC surfaces better than NMEC. (a) Representative images of cultured BCC and NMEC on gradient SAC surfaces. Scale bar, 8 μm. (b) Cell area, (c) cell aspect ratio, (d) FA number density polarization and (e) FA area polarization. Black asterisks (*) indicate significant differences between cell types for fibronectin, $p < 0.05$. X-axis in (d,e) shows the degree of polarization; negative and positive values represent polarization against and along the gradient direction, respectively.

Cell Morphology on Gradient SAC Surfaces. BCC and NMEC were cultured on gradient single active component (SAC) surfaces that were realized as fibronectin nanopatterns with spacing increasing from 1 to 10 μm on a K-casein background. Representative images are shown in Figure 5a. The areas of BCC on gradient SAC surfaces were smaller and larger than those on fibronectin and K-casein surfaces, respectively ($p < 0.05$) (Figure 5b). On the other hand, the areas of NMEC on gradient SAC surfaces were larger than both fibronectin and K-casein control surfaces ($p < 0.05$). In addition, NMEC occupied larger areas than BCC on gradient SAC surfaces ($p < 0.05$, *). In comparison to SAC surfaces with homogeneous 2, 4, or 8 μm spacing, areas of both cell types were larger on gradient SAC surfaces. For instance, the

average area of BCC was 539 ± 34 μm square on SAC surfaces with 2 μm spacing whereas it was 868 ± 36 μm square on gradient SAC surfaces. This could be due to more cells landing on areas with 1 μm spacing; however, this was not the case as cells were observed randomly on the gradient pattern. Therefore, gradient SAC surfaces appeared to enhance cell spreading especially for NMEC.

Aspect ratios of both cell types were not statistically different between control and gradient SAC surfaces. BCC were more asymmetric than NMEC on gradient SAC surfaces as well as on fibronectin control surfaces (Figure 5c). Aspect ratios of both cell types on gradient SAC surfaces were similar to those on homogeneous SAC surfaces. Thus, gradient SAC surfaces did not appear to drastically change aspect ratios of both cell types.

FAs on gradient SAC surfaces. On SAC surfaces, number densities of FAs for both cell types were polarized showing the presence of an inherent polarization (Supporting Information Figure S5a). Thus, when cell adhesion promoting regions were limited, cells could be more active in probing their microenvironment and polarizing their FAs. On gradient SAC surfaces, the number densities of FAs on fibronectin were polarized along the gradient direction for BCC but not NMEC. Thus, more FAs formed on fibronectin nanodots when the spacings between fibronectin nanodots were smaller (Figure 5d). This is in agreement with the number of FAs on SAC surfaces: the number of FAs on the fibronectin nanodots decreased as the spacing between fibronectin nanodots increased. Yet only BCC adapted to the gradient. On the other hand, NMEC formed more FAs on the K-casein background where the spacing between fibronectin nanodots were larger, presenting a negative polarization peak. BCC showed both positive and negative polarization peaks for number densities of FAs on the K-casein background. Thus, NMEC were more rigid in adaptation to SAC gradient surfaces whereas BCC exploit the gradient better by modulating number densities of FAs.

In contrast to fibronectin control surfaces, both cell types polarized areas of their FAs on fibronectin nanodots of SAC surfaces (Supporting Information Figures S4b and S5b). However, on gradient SAC surfaces the areas of FAs of BCC but not NMEC were larger on fibronectin nanodots with larger spacing (Figure 5e). This is in agreement with the result that the areas of FA on the fibronectin nanodots increased as the spacing between fibronectin nanodots increased on SAC surfaces. On gradient SAC surfaces, NMEC did not polarize the areas of FAs, suggesting inflexibility. The areas of FAs on the K-casein background were not polarized on homogeneous and gradient SAC surfaces in agreement with the result that areas of FAs were virtually constant for both cell types on the K-casein background of homogeneous SAC surfaces. Therefore, analysis of both number density and area of FAs showed that BCC but not NMEC adapted to and exploited gradient SAC surfaces by increasing the number and decreasing the areas of FAs on fibronectin nanodots with smaller spacing.

Cell Morphology on Gradient DAC Surfaces. BCC and NMEC were cultured on gradient double active component (DAC) surfaces that were realized as fibronectin nanopatterns with spacing increasing from 1 to 10 μm on a laminin background. Representative images are shown in Figure 6a. The cell areas of BCC on gradient DAC surfaces were smaller than those on fibronectin and similar to K-casein surfaces ($p < 0.05$) (Figure 6b). On the other hand, the areas of NMEC on gradient DAC surfaces were smaller than both fibronectin and laminin control surfaces ($p < 0.05$). In addition, NMEC occupied smaller areas than BCC on gradient DAC surfaces ($p < 0.05$, *). Furthermore, the areas of both cell types on gradient DAC surfaces were similar to those on DAC surfaces with 2, 4, or 8 μm spacing. These results suggested that gradients on DAC surfaces were not as effective as gradients on SAC surfaces for enhancing cell spreading. This was probably because cells explored further on SAC surfaces where cell adhesion promoting regions were limited.

Aspect ratios of both cell types were not statistically different between control and gradient DAC surfaces (Figure 6c). BCC were more asymmetric than NMEC on gradient DAC surfaces as well as on fibronectin control surfaces ($p < 0.05$). Aspect ratios of both cell types on gradient DAC surfaces were similar to those on homogeneous DAC surfaces. Thus, as was the case with the gradient SAC surfaces, the gradient DAC surfaces did not appear to radically change aspect ratios of both cell types.

FAs on Gradient DAC Surfaces. On laminin control and DAC surfaces, the number densities of FAs for both cell types were polarized showing the presence of an inherent polarization (Supporting Information Figures S4c and S6a). On gradient DAC surfaces, the polarization of number densities of FAs was along the gradient for both cell types on fibronectin nanodots (Figure 6d). This is in agreement with the number of FAs on DAC surfaces: the number of FAs on the fibronectin nanodots decreased as the spacing between fibronectin nanodots increased. Both cell types also formed more FAs on the laminin background where the spacing between fibronectin nanodots were smaller. This was in contrast to the result that the number of FAs on the laminin background of DAC surfaces increased as the spacing between fibronectin nanodots increased for both cell types. Here, polarization on fibronectin nanodots could be driving polarization on the laminin background. Comparing gradient SAC and gradient DAC surfaces, polarization of the number densities of FAs was different between NMEC and BCC only on gradient SAC surfaces where adhesive areas were limited.

The areas of FAs of BCC were not polarized on laminin control, homogeneous, or gradient DAC surfaces; the areas of FAs of NMEC were polarized only on the laminin background of DAC surfaces (Figure 6e, Supporting Information Figures S4b,d and S6b). This is in agreement with the fact that both fibronectin and laminin promote cell adhesion and the results on DAC surfaces suggesting that fibronectin was a better cell adhesion promoter than laminin for BCC but not NMEC. Thus, gradient DAC surfaces did not polarize areas of FAs for both cell types.

The most relevant study that we could find in the literature is a comparative study by Agus et al. in which BCC and NMEC were examined in various aspects.[12] One of the findings in that study was that NMEC preferred to adhere to hyaluronic acid micropatterns whereas BCC did not have a preference. Their results align with ours in that BCC appeared to act more independently than NMEC. Here, we quantitatively and comparatively analyzed adhesion of BCC and NMEC on protein nanopatterns and revealed that the number of FAs were the dominant parameter for regulation of cell adhesion.

Results on SAC surfaces showed significant differences in cell area, aspect ratio, and FA number and area between BCC and NMEC. The results were consistent with a more plastic phenotype for BCC. BCC occupied larger areas, decreased their asymmetry, and formed more and larger FAs on the K-casein background. NMEC appeared to require proper adhesive regions and did not adapt to the protein patterns. When introduced under flow to SAC surfaces, BCC adhered better than NMEC; their areas were larger and they formed more and smaller FAs. These results are expected because cancer cells are known to override regulations in multiple aspects and in adhesion as shown here. Furthermore, the observed adhesion phenotype of BCC under flow is likely to support their dissemination.

DAC surfaces enhanced cell adhesion for both BCC and NMEC. Both cell types occupied larger areas and formed more but smaller FAs on DAC compared to SAC surfaces. Yet, BCC formed more FAs than NMEC on fibronectin nanodots of DAC surfaces. Thus, BCC better adapted to and utilized DAC surfaces. Such adaptation is likely to favor cell survival.

The gradient surfaces confirmed results on homogeneous surfaces. In addition, the gradient SAC surfaces enhanced cell spreading for both cell types. Yet, BCC better exploited the
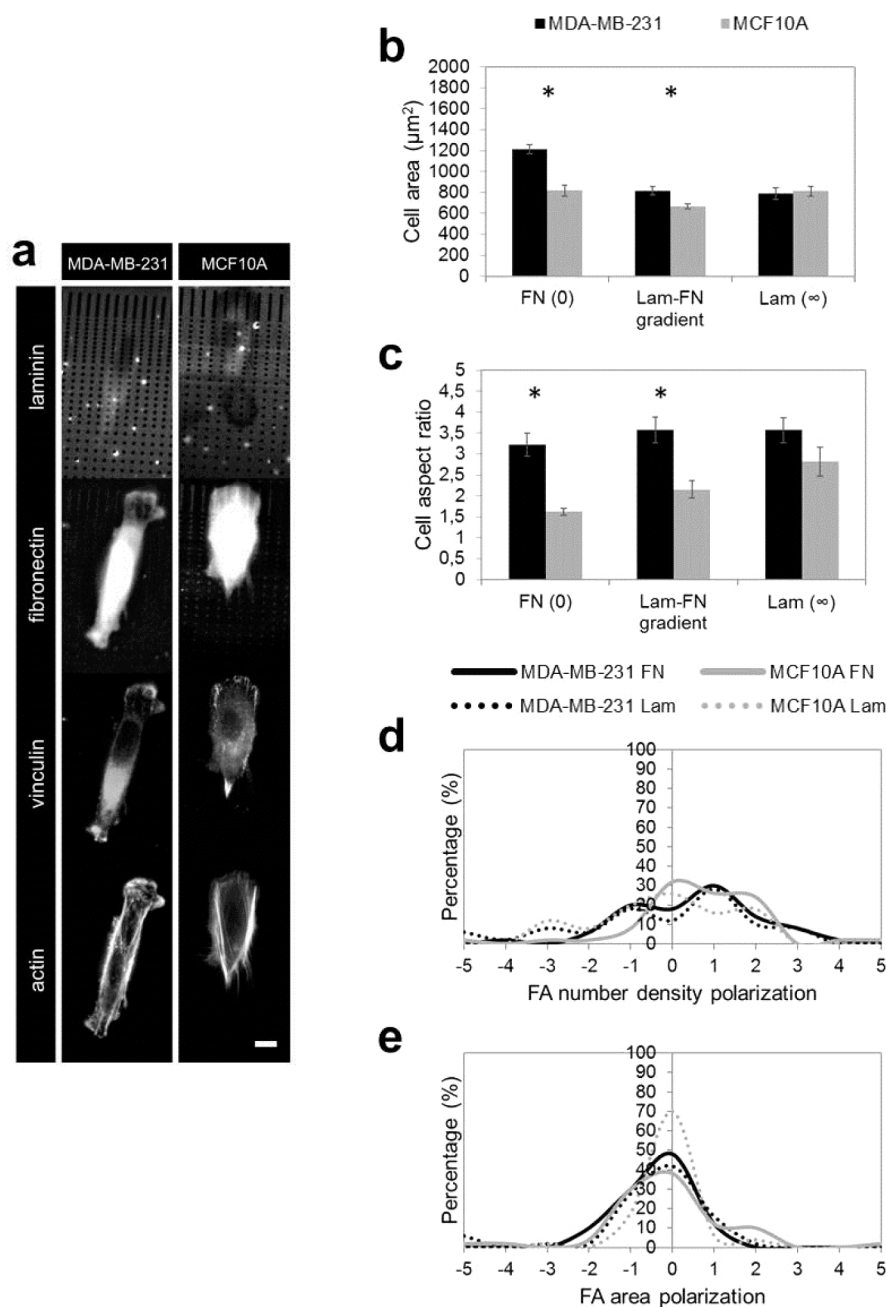
Figure 6. Both BCC and NMEC respond to gradient DAC surfaces similarly. (a) Representative images of cultured BCC and NMEC on gradient DAC surfaces. Scale bar, 8 μm. (b) Cell area, (c) cell aspect ratio, (d) FA number density polarization, and (e) FA area polarization. Black asterisks (*) indicate significant differences between cell types for fibronectin, $p < 0.05$. X-axis in (d,e) shows the degree of polarization; negative and positive values represent polarization against and along the gradient direction, respectively.

gradient by modulating the number and areas of FAs. Ability to respond to gradients enhances probably not only adhesion but migration and invasion as well because metastatic cells are likely to encounter gradients.

Conclusions. To the best of our knowledge, we have provided the first comparative and quantitative analysis of breast cancer and normal mammary epithelial cell adhesion on both single and double active, both homogeneous and gradient protein nanopatterns, under static and/or flow conditions. EBL is a powerful patterning technique to fabricate nano/micrometer scale surface patterns that mimic the in vivo organization of the extracellular matrix and thus provides an effective venue to compare adhesion of normal and cancerous cells. The results

showed that cell morphology was differentially modulated by normal and cancerous cells on custom designed protein patterns. In addition, cells regulated the number of FAs rather than the size of FAs in response to changes in the nano/micrometer scale organization of the surfaces. Interestingly, the total FA area per cell area was between 3 and 4% for all conditions. Thus, the differences in cell adhesion were determined by how cells allocated their resources and better adaptation came with regulating FA numbers rather than FA areas. Furthermore, differences between cell types were more evident on SAC surfaces where cell adhesion promoting areas were limited. Finally, BCC better adapted to polarization inducing conditions such as interstitial flow and gradient

surfaces demonstrating their plasticity. The nanopatterning approach presented here can be used to study changes in cell adhesion in different cancer cell lines. In conclusion, our findings offer exciting new opportunities for studies on cell adhesion, migration and extracellular matrix modification, comparing health and disease states.

Materials and Methods. Unless otherwise noted, materials were obtained from Sigma, Germany

Fabrication of Customized Protein Nanopatterns. K-casein coating of ITO-coated glass slides (TEKNOMA, Izmir, Turkey) was performed as previously described.[33] We used ITO-glass as a substrate because ITO-glass is both conductive, a requirement for EBL, and transparent. Silicon, a commonly used substrate for EBL, is not transparent and thus limits usage of many light microscopy-based assays used in cell biology.[33] In contrast to SAC, DAC surfaces were cultured with 0.025 mg/mL laminin instead of K-casein for 2 h. Each surface was patterned by EBL (Raith GmbH, Dortmund, Germany) using previously optimized parameters.[33] Uniform (2, 4, and 8 μm spaced dots) and gradient (1−10 μm spaced dots) patterns were designed using the Raith software in GDSII format. To systematically study the effect of the organization of ECM proteins, we chose spacing of 2, 4, and 8 μms. At spacing smaller than 1 μm, the patterning approach was not efficient due to proximity effects from the electron beam and the nature of the resists used, which were proteins. At a spacing of 8 μm, cell morphology and FA features were similar to those on K-casein surfaces. Therefore, larger spacing were not used. After EBL, SAC and DAC surfaces were backfilled with 0.05 mg/mL fibronectin or DyLight (Thermofisher Scientific, Waltham, MA) conjugated fibronectin for 2 h. Control samples contained only one type of protein: K-casein, fibronectin, or laminin.

Cell Culture. Unless otherwise noted, cell culture materials were obtained from Biological Industries, Israel. MDA-MB-231 cells were cultured in DMEM with 10% fetal bovine serum. MCF10A cells were cultured in DMEM/F12-HAM (1:1) supplemented with 5% donor horse serum, 20 ng/mL EGF, 500 ng/mL hydrocortisone, 100 ng/mL cholera toxin, and 0.01 mg/mL insulin. Cells were passaged every 2−3 days.

Under static conditions, cells were cultured in Leibovitz's medium (GIBCO/Invitrogen, Karlsruhe, Germany) for 2 h for basal metabolism. Subsequently, cells were lifted with 0.05% trypsin and cultured in their growth medium on SAC and\or DAC surfaces of ITO-glass with 1.8×10^6 cells per 100 mm Petri dish at 37 °C and 5% CO_2 for 18 h.

To apply a flow-induced shear stress, PDMS (polydimethylsiloxane) channel molds with 5 cm length, 13 mm width, and 960 μm height were UV/ozone treated and firmly placed on protein patterned ITO-glass slides and held together with butterfly paper clips. Flow was realized using a peristaltic pump. The flow rate was approximately 0.02 dyn/cm^2 in order to mimic interstitial flow. Trypsinized cells resuspended in Leibovitz's medium with 10% fetal bovine serum (FBS) were constantly stirred in a bottle using a magnetic stirrer. Cells were introduced via silicon tubing to the patterned surfaces of ITO-glass slides and recirculated for 24 h. The setup was kept at 37 °C using a water bath.

Immunofluorescence and Data Acquisition. Cells cultured on patterned surfaces were fixed with 4% paraformaldehyde in phosphate buffered saline (PBS) and permeabilized with 0.1% Triton X-100 in PBS. The samples were blocked with 1% bovine serum albumin and then incubated with vinculin and fibronectin or laminin specific primary antibodies, namely V9131, F3648, or

L9393. The samples were then labeled with the Alexa350, Alexa488, Alexa555, or Alexa647 fluorophore conjugated secondary antibodies and Alexa350 or 647 conjugated phalloidin that stains actin (Molecular Probes, Eugene, OR). Data in the form of fluorescence images were acquired by imaging the samples by an Olympus epifluorescence microscope with a 100× oil immersion objective.

Image Analysis. Image analysis was performed by ImageJ program. Focal adhesion analysis was performed as previously described.[40] Only single cells were analyzed to avoid contribution from cell−cell interactions. For polarization analysis, cell contours were manually drawn. Angle of the pattern was measured, and each cell was split into two regions designated as up (higher concentration of dots) and down (lower concentration of dots). Focal adhesions were separately analyzed in each part (Supporting Information Figure S7). Polarization for any parameter X was calculated as $Px = 5*[(X\text{up} - X\text{down})/(X\text{up} + X\text{down})]$. For homogeneous surfaces and static conditions, absolute value of Px was used.

Statistical Analysis. Data were processed by Excel. Outlier cells on the basis of cell area were excluded from the analysis. The number of cells per condition was in the range of $n = 7−66$ (Supporting Information Table S3). Student's t-test was used for statistical analysis. Results were presented as mean $\pm$ standard error.

■ ASSOCIATED CONTENT

ⓢ Supporting Information

Additional information and figures. The Supporting Information is available free of charge on the ACS Publications website at DOI: 10.1021/acs.nanolett.5b01785.

■ AUTHOR INFORMATION

Corresponding Author
*E-mail: devrimpesen@iyte.edu.tr.

Author Contributions
U.H. and B.O. contributed equally to this work.

Notes
The authors declare no competing financial interest.

■ REFERENCES

(1) Kim, D.-H.; Provenzano, P. P.; Smith, C. L.; Levchenko, A. *J. Cell Biol.* **2012**, *197* (3), 351−360.

(2) Soucy, P. A.; Romer, L. H. *Matrix Biol.* **2009**, *28* (5), 273−283.

(3) Wolf, K.; Alexander, S.; Schacht, V.; Coussens, L. M.; von Andrian, U. H.; van Rheenen, J.; Deryugina, E.; Friedl, P. *Semin. Cell Dev. Biol.* **2009**, *20* (8), 931−941.

(4) Zoumi, A.; Yeh, A.; Tromberg, B. J. *Proc. Natl. Acad. Sci. U. S. A.* **2002**, *99* (17), 11014−11019.

(5) Provenzano, P. P.; Eliceiri, K. W.; Keely, P. J. *Clin. Exp. Metastasis* **2009**, *26* (4), 357−370.

(6) Gattazzo, F.; Urciuolo, A.; Bonaldo, P. *Biochim. Biophys. Acta, Gen. Subj.* **2014**, *1840* (8), 2506−2519.

(7) Berginski, M. E.; Vitriol, E. A.; Hahn, K. M.; Gomez, S. M. *PLoS One* **2011**, *6* (7), e22025.

(8) Berrier, A. L.; Yamada, K. M. *J. Cell. Physiol.* **2007**, *213* (3), 565–573.

(9) Zaidel-Bar, R.; Cohen, M.; Addadi, L.; Geiger, B. *Biochem. Soc. Trans.* **2004**, *32* (Pt3), 416–420.

(10) Lu, P.; Weaver, V. M.; Werb, Z. *J. Cell Biol.* **2012**, *196* (4), 395–406.

(11) Agheli, H.; Malmstrom, J.; Larsson, E. M.; Textor, M.; Sutherland, D. S. *Nano Lett.* **2006**, *6* (6), 1165–1171.

(12) Agus, D. B.; Alexander, J. F.; Arap, W.; Ashili, S.; Aslan, J. E.; Austin, R. H.; Backman, V.; Bethel, K. J.; Bonneau, R.; Chen, W. C.; Chen-Tanyolac, C.; Choi, N. C.; Curley, S. A.; Dallas, M.; Damania, D.; Davies, P. C.; Decuzzi, P.; Dickinson, L.; Estevez-Salmeron, L.; Estrella, V.; Ferrari, M.; Fischbach, C.; Foo, J.; Fraley, S. I.; Frantz, C.; Fuhrmann, A.; Gascard, P.; Gatenby, R. A.; Geng, Y.; Gerecht, S.; Gillies, R. J.; Godin, B.; Grady, W. M.; Greenfield, A.; Hemphill, C.; Hempstead, B. L.; Hielscher, A.; Hillis, W. D.; Holland, E. C.; Ibrahim-Hashim, A.; Jacks, T.; Johnson, R. H.; Joo, A.; Katz, J. E.; Kelbauskas, L.; Kesselman, C.; King, M. R.; Konstantopoulos, K.; Kraning-Rush, C. M.; Kuhn, P.; Kung, K.; Kwee, B.; Lakins, J. N.; Lambert, G.; Liao, D.; Licht, J. D.; Liphardt, J. T.; Liu, L.; Lloyd, M. C.; Lyubimova, A.; Mallick, P.; Marko, J.; McCarty, O. J.; Meldrum, D. R.; Michor, F.; Mumenthaler, S. M.; Nandakumar, V.; O'Halloran, T. V.; Oh, S.; Pasqualini, R.; Paszek, M. J.; Philips, K. G.; Poultney, C. S.; Rana, K.; Reinhart-King, C. A.; Ros, R.; Semenza, G. L.; Senechal, P.; Shuler, M. L.; Srinivasan, S.; Staunton, J. R.; Stypula, Y.; Subramanian, H.; Tlsty, T. D.; Tormoen, G. W.; Tseng, Y.; van Oudenaarden, A.; Verbridge, S. S.; Wan, J. C.; Weaver, V. M.; Widom, J.; Will, C.; Wirtz, D.; Wojtkowiak, J.; Wu, P. H. *Sci. Rep.* **2013**, *3*, 1449.

(13) Alsberg, E.; Feinstein, E.; Joy, M. P.; Prentiss, M.; Ingber, D. E. *Tissue Eng.* **2006**, *12* (11), 3247–3256.

(14) Biggs, M. J.; Richards, R. G.; Dalby, M. J. *Nanomedicine* **2010**, *6* (5), 619–633.

(15) Cavalcanti-Adam, E. A.; Volberg, T.; Micoulet, A.; Kessler, H.; Geiger, B.; Spatz, J. P. *Biophys. J.* **2007**, *92* (8), 2964–2974.

(16) Chen, C. S.; Mrksich, M.; Huang, S.; Whitesides, G. M.; Ingber, D. E. *Science* **1997**, *276* (5317), 1425–1428.

(17) Elineni, K. K.; Gallant, N. D. *Biophys. J.* **2011**, *101* (12), 2903–2911.

(18) Gingras, J.; Rioux, R. M.; Cuvelier, D.; Geisse, N. A.; Lichtman, J. W.; Whitesides, G. M.; Mahadevan, L.; Sanes, J. R. *Biophys. J.* **2009**, *97* (10), 2771–2779.

(19) Li, J. R.; Shi, L.; Deng, Z.; Lo, S. H.; Liu, G. Y. *Biochemistry* **2012**, *51* (30), 5876–5893.

(20) Lutz, R.; Pataky, K.; Gadhari, N.; Marelli, M.; Brugger, J.; Chiquet, M. *PLoS One* **2011**, *6* (9), e25459.

(21) Malmstrom, J.; Lovmand, J.; Kristensen, S.; Sundh, M.; Duch, M.; Sutherland, D. S. *Nano Lett.* **2011**, *11* (6), 2264–2271.

(22) Oliva, A. A., Jr.; James, C. D.; Kingman, C. E.; Craighead, H. G.; Banker, G. A. *Neurochem. Res.* **2003**, *28* (11), 1639–1648.

(23) JinSeok, P.; Hong-Nam, K.; Deok-Ho, K.; Levchenko, A.; Kahp-Yang, S. *NanoBioscience, IEEE Transactions on* **2012**, *11* (1), 28–36.

(24) Pesen, D.; Haviland, D. B. *ACS Appl. Mater. Interfaces* **2009**, *1* (3), 543–548.

(25) Hanahan, D.; Weinberg, R. A. *Cell* **2011**, *144* (5), 646–674.

(26) Desgrosellier, J. S.; Cheresh, D. A. *Nat. Rev. Cancer* **2010**, *10* (1), 9–22.

(27) Liotta, L. A.; Kohn, E. C. *Nature* **2001**, *411* (6835), 375–379.

(28) Stetlerstevenson, W. G.; Aznavoorian, S.; Liotta, L. A. *Annu. Rev. Cell Biol.* **1993**, *9*, 541–573.

(29) Rundqvist, J.; Mendoza, B.; Werbin, J. L.; Heinz, W. F.; Lemmon, C.; Romer, L. H.; Haviland, D. B.; Hoh, J. H. *J. Am. Chem. Soc.* **2007**, *129* (1), 59–67.

(30) Kim, S.; Marelli, B.; Brenckle, M. A.; Mitropoulos, A. N.; Gil, E.-S.; Tsioris, K.; Tao, H.; Kaplan, D. L.; Omenetto, F. G. *Nat. Nanotechnol.* **2014**, *9* (4), 306–310.

(31) Pesen, D.; Heinz, W. F.; Werbin, J. L.; Hoh, J. H.; Haviland, D. B. *Soft Matter* **2007**, *3* (10), 1280–1284.

(32) Kolodziej, C. M.; Maynard, H. D. *Chem. Mater.* **2012**, *24* (5), 774–780.

(33) Horzum, U.; Ozdil, B.; Pesen-Okvur, D. *Mater. Res. Express* **2014**, *1* (2), 025402.

(34) Akkiprik, M.; Nicorici, D.; Cogdell, D.; Jia, Y. J.; Hategan, A.; Tabus, I.; Yli-Harja, O.; Yu, D.; Sahin, A.; Zhang, W. *Technol. Cancer Res. Treat.* **2006**, *5* (6), 543–551.

(35) Brenton, J. D.; Carey, L. A.; Ahmed, A. A.; Caldas, C. *J. Clin. Oncol.* **2005**, *23* (29), 7350–7360.

(36) Cailleau, R.; Mackay, B.; Young, R. K.; Reeves, W. J. *Cancer Res.* **1974**, *34* (4), 801–809.

(37) Debnath, J.; Muthuswamy, S. K.; Brugge, J. S. *Methods* **2003**, *30* (3), 256–268.

(38) Plopper, G. E.; Domanico, S. Z.; Cirulli, V.; Kiosses, W. B.; Quaranta, V. *Breast Cancer Res. Treat.* **1998**, *51* (1), 57–69.

(39) Pedersen, J. A.; Boschetti, F.; Swartz, M. A. *J. Biomech.* **2007**, *40* (7), 1484–1492.

(40) Horzum, U.; Ozdil, B.; Pesen-Okvur, D. *MethodsX* **2014**, *1*, 56–59.

■ NOTE ADDED AFTER ASAP PUBLICATION

This paper was published on the Web on July 7, 2015, with the incorrect artwork for Figures 2–4. The corrected version was reposted on July 8, 2015.